



# Synthesis of anatase nanoparticles with enhanced photocatalytic performance by using microfluidic method

Wu Zhang<sup>1</sup> · Yanhui Hua<sup>2</sup>

Received: 5 December 2022 / Accepted: 15 February 2023 / Published online: 25 February 2023  
© Institute of Chemistry, Slovak Academy of Sciences 2023

## Abstract

Anatase nanoparticles (NPs) are physiochemically elusive during preparation due to their agglomeration-oriented behavior, which can significantly decrease their photocatalytic properties. Herein, we are proposing a microfluidic method to synthesize anatase nanoparticles with enhanced photocatalytic performance by using  $\text{TiCl}_4$  and absolute ethyl alcohol–water mixture as the starting material and solvent. The preparation process is experimentally investigated by using  $L_{25}(5^6)$  orthogonal method. The results indicate that residence time is the key factor for particle size of anatase NPs. The as-synthesized samples are characterized by a high-resolution transmission electron microscope and X-ray diffractometer as well as a laser particle size analyzer. The isoelectric points of the as-prepared samples range from 6 to 7, and they exhibit smaller agglomeration and higher adsorption capacity than commercial P-25. Of particular to this study is the quantitative evaluation on effects of the factors on photocatalytic activities of the samples and the interactions between the factors by using response surface methodology (RSM). The as-synthesized anatase NPs exhibit much higher photocatalytic activities than commercial P-25 and the nanostructured anatase reported in the previous literature.

**Keywords** Anatase nanoparticles · Photocatalytic performance · Microfluidic method

## Introduction

$\text{TiO}_2$  has been commercially used as a typical photocatalyst over the last decades (Monfared and Jamshidi 2019). It naturally forms in four main phases: rutile, anatase, brookite, and  $\text{TiO}_2(\text{B})$  (Cargnello et al. 2014). Among them, anatase has gained extensive attention in the field of organic pollutant degradation due to its high photocatalytic activity (Lin et al. 2011; Gautam et al. 2016; Gao et al. 2015; Done et al. 2010). Additionally, nanoscaled  $\text{TiO}_2$  structures normally exhibit higher physicochemical properties than those on a micro-sized scale (Zhou et al. 2006; Tabaei et al. 2012). However, nanostructured  $\text{TiO}_2$  is physiochemically elusive due to its agglomeration-oriented behavior. Therefore, a controllable synthesis process is a prerequisite for gaining the desirable

characteristics of the final material. The methods for preparing  $\text{TiO}_2$  nanomaterials can be divided into physical and chemical methods (Chen and Mao 2007). Physical methods are normally associated with top–down approaches in which small structures are fabricated from larger ones (Chen and Mao 2007; Dubey and Singh 2017). In contrast, chemical methods proceed through a bottom–up approach in which the molecules react to form the final larger structures (Chen and Mao 2007). The wet chemical method is one of the most convenient and popular chemical methods to synthesize  $\text{TiO}_2$  nanostructures, simply because it provides the possibility of precise control of the quality of products (Cargnello et al. 2014).  $\text{TiO}_2$  with various morphology, e.g. thin films, tubes, and rods have been prepared in a range of Ti-containing solutions (Chen and Mao 2007). Yuenyongsuwan et al. (2018) synthesized  $\text{TiO}_2$  NPs by microemulsion and hydrothermal methods using titanium tetra-isopropoxide as a precursor; they reported that the size and phase of  $\text{TiO}_2$  NPs can be controlled by adding surfactant micelle and varying operation parameters like pH and temperature, while other information of their products was not given in details. Jinju Zhang et al. (2018) developed a microwave-assisted method to prepare  $\text{TiO}_2$  NPs by fast hydrolysis of inorganic titanyl sulfate and post-annealing treatment at 700 °C;

✉ Wu Zhang  
neusmmzhangwu@163.com

<sup>1</sup> School of Materials Science and Engineering, Shenyang Ligong University, Shenyang, Liaoning 110159, People's Republic of China

<sup>2</sup> Engineering Training Center, Shenyang Ligong University, Shenyang, Liaoning 110159, People's Republic of China

they obtained  $\text{TiO}_2$  agglomerates of  $< 10$  nm crystalline powders. Dar et al. (2014) published their work on a rapid and facile synthesis of  $\sim 7$  nm and 100–400 nm nanostructures of anatase by exploiting the chemical nature of solvents through a microwave-based approach. Another study presented by László Kőrösia et al. (2018) demonstrated that hydrothermal treatment increases the particle size and the crystallinity of  $\text{TiO}_2$  NPs, while the morphology did not change significantly. Nithya et al. (2018) synthesized  $\text{TiO}_2$  and Nd-doped  $\text{TiO}_2$  NPs with an average crystallite size of 10–14 nm through a sol–gel method, and it was reported that Nd had a critical effect on phase transition of  $\text{TiO}_2$  NPs.

To date, a major challenge with the synthesis of  $\text{TiO}_2$  NPs is the lack of control over the synthesis process. The microfluidic method has been used for various applications in the field of chemical engineering and sustainable chemistry. Compared to conventional devices, microfluidic devices are composed of microfabricated components like micromixers, microchannels, microtubes, etc. (Priest et al. 2011). Efficient mass transfer can be easily achieved (Jiang et al. 2018; Yin et al. 2018; Chen et al. 2019), which makes the microfluidic method well suited for synthesis of materials. Diverse of experimental apparatus have been developed for preparing materials with desired properties (Bendre et al. 2022). A prime example is that microfluidic method has been proved to be an alternative for fabrication of NPs or spheres with desirable morphology and properties (Li et al. 2022; Chen et al. 2022; Mou et al. 2022; Pandit et al. 2022). Additionally, the chemical reactions in the microreactors can be controlled much easier than that in the batch synthesis of materials, and the precision of the preparation of small (e.g.,  $< 100$  nm and often  $< 10$  nm) structures by microfluidic can approach the atomic-layer limit (Pei et al. 2018; He et al. 2018).

Inspired by the advantages of the microfluidic method, we design a microfluidic flow cell to achieve precise control over the synthesis of anatase NPs. Additionally, we introduce a water–absolute ethyl alcohol mixture as the solvent, which is critical for controlling the hydrolysis rate of  $\text{TiCl}_4$  in the microchannels. The resulting anatase NPs are characterized using HRTEM to gain insight into the growth of the NPs in the microreactor. The behavior of anatase NPs in aqueous suspensions is discussed in terms of zeta potential and agglomerate size. Moreover, response surface methodology is performed to assess the effect of each factor on the degradation process of phenol.

## Experimental

### Materials

$\text{TiCl}_4$ , deionized water, and absolute ethyl alcohol serve as the starting materials, in which absolute ethyl alcohol was

used as inhibitor to diminish the hydrolysis rate of  $\text{TiCl}_4$  in water in order to better control the reaction rate in the microreactor. NaOH is used to adjust the pH of the water–absolute ethyl alcohol mixture. All the chemicals, as mentioned above, are purchased from Sinopharm Chemical Reagent Co., Ltd., China, and they are used as received. Commercial  $\text{TiO}_2$  powder (Aeroxide P-25) is purchased from Evonik-Degussa.

### Experimental setup and synthesis of anatase NPs

Figure 1 shows the schematic diagram of the synthesis process. The experimental setup consists of two micro syringe pumps (PHD Ultra, Harvard Apparatus) and a microreactor, which is designed by our group (commissioned by Shenyang Zhongshan Precision Instrument Co., Ltd. to manufacture). The microreactor is mainly composed of a Y-junction chip ( $30 \times 30 \times 5$  mm) with ten round microchannels, which are embedded in stainless steel modules, is employed to perform the experiments. The microchannels distribute uniformly in the chips with a spacing of 2 mm. Herein, the width of the microchannel should be designed properly. Narrow channel leads to blocking of the microchannel, while excessive width of the microchannel commonly renders low controllability of the reactions. The channel width can be varied by changing the modules. Five chips with different widths of microchannel ranging from 100 to 180  $\mu\text{m}$  with an increment of 20  $\mu\text{m}$  are used in the present work. The residence time could be controlled by changing the injection rate of  $\text{TiCl}_4$  and solvent. The water–absolute ethyl alcohol mixture serves as the reaction medium, and the volume fraction of absolute ethyl alcohol is within the range of 0.5–0.9. The mixture in the microchannels is heated using an oil bath. The synthesis temperatures varied from 50  $^\circ\text{C}$  to 130  $^\circ\text{C}$ . Typically,  $\text{TiCl}_4$  and water–absolute ethyl alcohol mixture (injection rate of  $\text{TiCl}_4$ : water: absolute ethyl alcohol = 1:2:7) are introduced

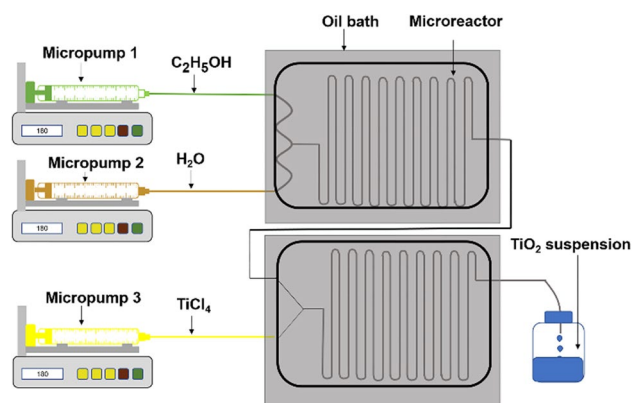


**Fig. 1** Schematic of the apparatus for microfluidic synthesis of anatase NPs

into the microchannels by two pumps, followed by an entry into the Y-junction inlets, and pass through the channels.

For the synthesis of anatase NPs, briefly, prior to synthesis experiments, the pH of water is adjusted to 12 using NaOH solution (concentration 0.1 mol/L) and the channel width is set at 200  $\mu\text{m}$ , and then  $\text{TiCl}_4$ , deionized water as well as alcohol are injected into the microreactors in the manner as shown in Fig. 1, the injection rates of  $\text{TiCl}_4$  and water are controlled at 0.1 and 0.3 mL/min, respectively. The temperature is set at 90 °C. Afterward, the mixture is centrifuged at 19,000 rad/min to separate the NPs from suspension.

### Sample characterization

A high-resolution transmission electron microscope (HRTEM, KEM-ARM200F, JEOL Ltd. Tokyo, Japan) is operated at 200 kV to observe the morphologies and crystal plane distances of the resulting anatase NPs. Before observation, a 2.5 wt% suspension of the prepared sample is dispersed in absolute ethyl alcohol for 5 min using ultrasound instrument (FS-450, Shenxi Ultrasound Instruments, Shanghai, China). Then, the suspension is deposited on a carbon-coated copper grid (Zhongjing Scientific Instrument, Beijing, China) and dried in an oven at 323 K for 20 min before loading into a single tilt holder. The particle sizes of the products are determined by a laser particle analyzer (Zetasizer Nano S90, Malvern Instruments Ltd., UK). The zeta potential and size of the aggregates obtained in aqueous suspensions are measured with the help of a Zetasizer. The samples are also characterized using a Philip X pert machine (MPDDY2094, Netherlands) with copper  $K\alpha$  irradiation ( $\lambda = 1.5406$  nm), at an operating voltage of 30 kV and a scanning angle within a scanning range 10–90°. XRD patterns of the samples are analyzed by X-pert high score plus software.

### Design of experiments

Effects of operating parameters including pH (factor A), residence time (factor B), channel width (factor C), temperature (factor D), and ratio of alcohol in absolute water–ethyl alcohol mixture (factor E) on the particle size of anatase NPs are investigated using  $L_{25}(5^6)$  orthogonal experimental method. The surface response methodology is employed to investigate the degradation of phenol. Degradation time,  $\text{TiO}_2$  dosage, degradation temperature, and pH are selected as four key factors, and they are varied in the range of 20–40 min, 150–250 mg/L, 25–30 °C, and 5–7, respectively.

### Photocatalytic activity test

Before the photocatalytic activity test, the mixture of  $\text{TiO}_2$  NPs and phenol solution is stirred in the dark for 10 min to minimize the effect of adsorption. To test the photocatalytic activity of the  $\text{TiO}_2$  nanoparticles, a 400 W high-pressure mercury lamp (HL400EH-5, SEN, Japan) with its spectra range from 253.7 to 577 nm was used as the light source. The photonic efficiency can be found in the literature (Wang et al. 2002). The distance from the lamp to the solution is 10 cm. Typically, 50 mg  $\text{TiO}_2$  is added to a 250 mL phenol solution (50 mg/L), which is placed in a 500 mL quartz beaker to test the activity of the samples. We adjust the pH by  $\text{H}_2\text{SO}_4$  (1:1) or NaOH solutions (0.5%) using a pH meter. Then the suspension is stirred and kept in the dark for 120 min to establish adsorption–desorption equilibrium. Afterward, the lamp is kept open in the photocatalytic degradation process, 3 mL slurry is taken out of the beaker every 10 min and subsequently centrifuged, high-performance liquid chromatography (Thermo Fisher UltiMate3000) with C18 column and PDA detector (SPD-M20A, SHIMADZU) is used to determine phenol concentration. To determine the phenol concentration in the degraded solution, 1.0 mL standard solution is placed in a centrifuge tube and then mixed with methanol to 5 mL. One milliliter of degraded phenol solution is placed in another centrifuge tube, and acetonitrile and water are served as mobile phase at a flow rate of 1.0 mL/min. Twenty microliters of sample is introduced at a wave of 280 nm. The peak areas of standard and test solutions are obtained to calculate the concentration of phenol in the degraded solution. The calibration range for identifying phenol in the present work is 0.01–0.2 g/L.

## Results and discussion

### Sample characterization

Figure 2 shows the XRD patterns of the samples. All the prepared samples are anatase, other phases of  $\text{TiO}_2$ , such as rutile and brookite, are not detected. The samples in Fig. 2 possess different peak intensities. However, in the case of liquid synthesis, peak intensity can change upon various factors, e.g., pH of the solution and experimental temperature. To study the effect of pH on the peak intensity of the samples (b, c, and d in Fig. 2), we prepare the samples under the same condition but with increased pH. Interestingly, the crystallinity degrees of the b, c, and d increase with pH, which indicates that higher pH can enhance the crystallization of the anatase crystals effectively. For example, the intensities of (101) plane are 2432, 2562, and 6608 for the samples at pH 10, 11, and 13. Testino et al. (2007) explained this phenomenon; they reported that large quantities of

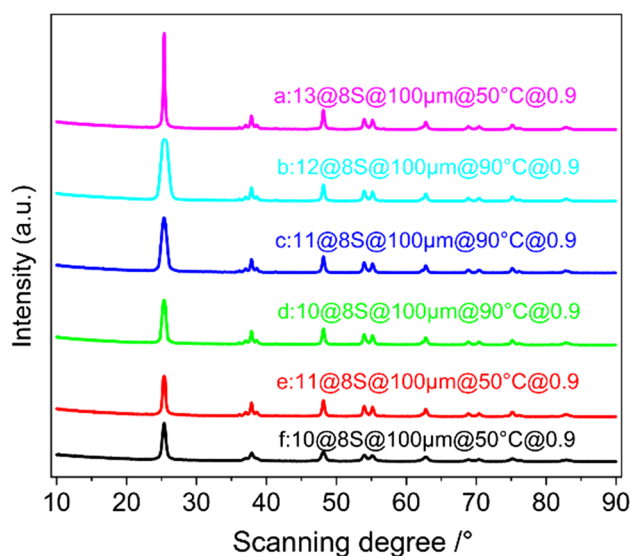


**Fig. 2** XRD patterns of the prepared samples (Note pH @ residence time @ temperature channel width @  $\text{TiCl}_4$  injection rate)

hydroxide ions can enhance the probability of edge-sharing structure at high pH, which is conducive to the formation of anatase. At low pH, on the other hand, more water molecules are bound to the  $\text{Ti}^{4+}$  center, which favors corner-sharing and leads to the formation of rutile  $\text{TiO}_2$ . This agrees with the experimental results in the present work. Dambournet et al. (2010) found that chloride anion act as a strong complexing agent, which leads to a poorly crystallized anatase phase. However, we still obtain highly crystallized anatase in the present work, which may arise from the presence of ethyl alcohol.

To seek more information on the synthesized samples, we perform the morphology and size distribution studies on the samples shown in Fig. 2a e and f, i.e., effect of pH on the morphologies of the samples, and the results shown in Fig. 3. As observed by the HRTEM and determined by the particle size analyzer, the particle size of the sample at pH 10 is about 40 nm (Fig. 3a), with the increase of pH to 11–13, the particles grow to 50–60 nm, indicating that higher pH is conducive to growth of anatase NPs. To confirm this information, particle size distribution of the samples shown in Fig. 3 are tested by using laser particle size analyzer, and the results are shown in Fig. S1 to S3. The average particle size of the samples shown in Fig. 3a, b and c are determined to be 42 nm, 49 nm, and 61 nm, which is close to the HRTEM observation results.

### Effect of operating parameters on the particle size of the as-prepared $\text{TiO}_2$ nanoparticles

Particle size plays a decisive on the performance of the samples. Indeed, several factors can influence the particle size

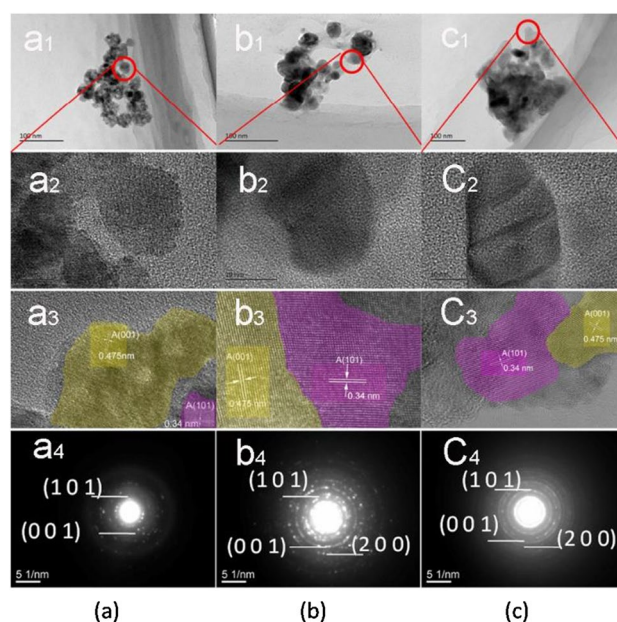


**Fig. 3** HRTEM images of the prepared samples with different pH values (pH of  $\mathbf{a}_1$ ,  $\mathbf{b}_1$  and  $\mathbf{c}_1$  13, 11, 10;  $\mathbf{a}_2$ ,  $\mathbf{b}_2$  and  $\mathbf{c}_2$  HRTEM images of individual nanoparticles;  $\mathbf{a}_3$ ,  $\mathbf{b}_3$  and  $\mathbf{c}_3$  typical area of (1 0 1) and (0 0 1) planes of anatase;  $\mathbf{a}_4$ ,  $\mathbf{b}_4$  and  $\mathbf{c}_4$  electron diffraction patterns of  $\mathbf{a}_1$ ,  $\mathbf{b}_1$  and  $\mathbf{c}_1$ )

of anatase nano-crystallites. As known to all, the orthogonal experimental method is a powerful tool to quantize the effect of each variable on a function value.  $L_{25}(5^6)$  orthogonal experiments are performed to assess the effect of each factor on particle size. Table S1 outlines the schedule of the orthogonal tests used to assess the key factors, pH (factor A), residence time (factor B), channel width (factor C), temperature (factor D) and the ratio of alcohol in water–absolute ethyl alcohol mixture (factor E) are selected as the five variable factors. The orthogonal experimental details are shown in table S2, and the results are listed in Table 1.

In Table 1, two important parameters are used to evaluate the significance of the factors, namely  $K_i$  and  $R_j$ .  $K_i$  is the average value of the sum of experimental results at the same level of each factor. It can be used to determine the optimal value of each factor.  $R_j$  is denoted as the difference between the maximum and minimum value of  $K_i$ . Smaller particles are desired products. The  $K$  values in Table 1 indicate that the optimal operating parameters for the minimum particle size of anatase NPs are:  $A_4$ ,  $B_1$ ,  $C_4$ ,  $D_3$ , and  $E_2$ . The significance order of the factors can be determined by comparing the  $R$  values of the factors, the  $R$  values of the factors follow the trend:  $R_B(50.6) > R_A(24.8) > R_D(11) > R_C(10) > R_E(9.4)$ , indicating that factor B (residence time) is the most significant factor for particle size of the products. Thermodynamically, a larger residence time is conducive to particle growth. Unlike the experiments in conventional batch synthesis, the



**Table 1** Results of  $L_{25}(5^6)$  orthogonal experiments

	A	B	C	D	E
$K_1$	72.6	29.4	57.6	56.4	63.8
$K_2$	64.6	44	59.2	65.8	54.4
$K_3$	55.8	62.6	65.4	54.8	57.8
$K_4$	47.8	79.2	55.4	59.2	59.4
$K_5$	55.2	80	58.4	59.8	60.6
$R$	24.8	50.6	10	11	9.4

The particle size is measured by laser particle size analyzer;  $K_i$  is the average value of the experimental results at the same level.  $R_j$  is the D-value of the maximum and minimum values of  $K_i$

mixture in the microchannels is not stirred but flows in the same direction, which makes it provides a better mass transfer for the growth of individual particles. In the situation of batch experiments, there is a higher probability of colliding between small particles and the larger ones, which would be a result of particle agglomeration. To provide more information on particle size of the  $\text{TiO}_2$  NPs, the dependence of the particle size of the  $\text{TiO}_2$  NPs on flow rate of  $\text{TiCl}_4$  with fixed flow rate of solvent is studied, the results are shown in Fig. S4. Exponential growth of the particle size is observed with the increasing of flow rate.

### Behavior of anatase NPs in water

A lot of research results imply that surface-dependent mechanisms can be used to describe the photocatalytic degradation of organic pollutants in aqueous solutions (Lin et al. 2011; Gautam et al. 2016; Gao et al. 2015; Dong et al. 2010). Consequently, particle agglomeration and surface charges play key roles in the surface chemistry of photodegradation processes. Two synthesized samples, named as Anatase-25, Anatase-40, and P-25, which represent the anatase samples of 25 nm and 40 nm are selected to investigate the behavior of  $\text{TiO}_2$  nano-powders in water (150 mg/L). Additionally, commercial P-25 is used as the comparative sample to better understand the behavior of anatase NPs in suspensions. The zeta potential and agglomeration size of the sample in water are shown in Fig. 4. Of note, fluid–structure interaction (FSI) problems in microchannels is influential on particle size of the  $\text{TiO}_2$  NPs, which may lead to the unregular trend part of the curve in Fig. 4.

The relationships between pH and the corresponding zeta potential are plotted in Fig. 4a. Positive zeta potentials are detected at low pH, while a negative value of zeta potential is observed with the increasing of pH. As a result, there is a specific pH corresponding the zero zeta potential, which is called isoelectric pH. The isoelectric pH of the two synthesized anatase samples locate between 6 and 7, while it is close to 5 for the sample of P-25 (Fig. 4a).

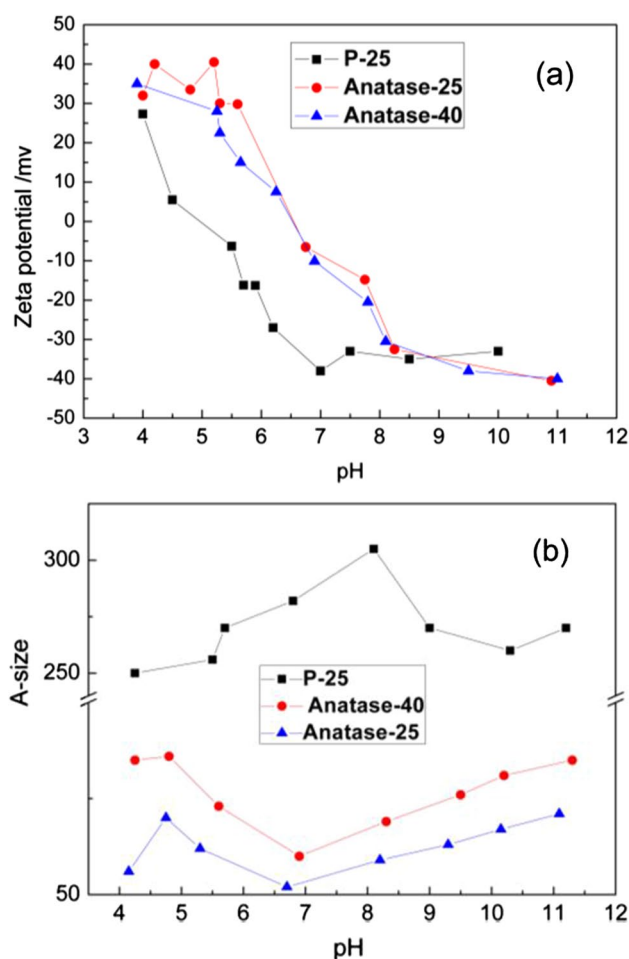


**Fig. 4** pH versus zeta potential and agglomeration size of the nano-powders in water (**a** zeta potential, **b** agglomeration size versus pH; Anatase-25 and Anatase-40 represent particles of 25 nm and 40 nm, respectively)

The agglomeration size of P-25 (282 nm) is much larger than the other two samples at pH 7 (52 nm and 60 nm for Anatase-25 and Anatase-40, Fig. 4b). Table 2 summarizes the characteristics of the synthesized anatase nanoparticles in aqueous suspensions. Compared with the two anatase samples, P-25 possesses a larger agglomeration size.

As mentioned above, the behavior of anatase NPs in water is critical to their photocatalytic performance. According to the results presented in Fig. 4, the Anatase-25 could possess better photocatalytic performance than the other two samples. To confirm this information, UV–Vis spectrum of the samples is performed (Fig. S5). It is shown that P25 mainly responds to the ultraviolet light region. In contrast, the samples Anatase-25 and Anatase-40 show significant absorption in visible light region. Additionally, compared with Anatase-40, the sample of Anatase-25 shows better visible light absorption property. To study the photocatalytic activity of the samples, we choose a phenol solution at a pH

**Table 2** Characteristics of the synthesized anatase nano-powders and P-25 in aqueous suspensions at isoelectric pH

No.	Ph	Particle size (nm)	Agglomeration size (nm)	Accessible surface ( $\text{m}^2 \text{g}^{-1}$ )
Anatase-25	6.7	25	52	29.62
Anatase-40	6.9	40	60	25.67
P-25	6.8	25	282	5.46

Anatase-25 and Anatase-40 represent anatase NPs of 25 nm and 40 nm, P-25 represent the commercial  $\text{TiO}_2$  nano-powder

of 6.8 to test the photocatalytic activities of the samples. Prior to degradation, the intrinsic sorption capacities of the selected samples are measured using phenol solution in dark conditions to remove the effect of adsorption of phenol in the solution. The results are shown in Fig. 5a. In Fig. 5a; after 2 min of adsorption, it is found that Anatase-25 possesses a higher tolerance capacity of phenol than Anatase-40 and commercial P-25. This attributes to the larger specific area of Anatase-25. After adsorption, the results of photocatalytic degradation tests of phenol are compared in Fig. 5b. As expected, the sample Anatase-25 exhibits higher photocatalytic activity than other samples for phenol degradation. Compared with P-25, the synthesized samples showed higher photocatalytic activity due to their larger specific surface areas. Additionally, the photocatalytic activities of the samples are not influenced by the adsorption of phenol in the solution. Powder surface area is directly related to primary particle size, aggregate size, and degree of dispersion. Additionally, anatase is known to be the most efficient  $\text{TiO}_2$  for photocatalytic applications, while P-25 possesses a mixed structure of anatase and rutile, which makes it a lower efficiency photocatalyst than pure anatase.

### Photocatalytic activity evaluation using response surface methodology

The degradation process of phenol is quite complex, and it is challenging to assess the photocatalytic activity of the synthesized samples by single-factor experiments. The optimization of the degradation process is extremely difficult when more than two factors are varied simultaneously. Some further investigations are necessary to overcome this problem. The Box–Behnken design (BBD) is an ideal method for catalytic reactions. According to this method, the experimental times can be represented as (Lujan et al. 2018; Zhang et al. 2017):

$$N = 2^k(k - 1) + C_0 \quad (1)$$

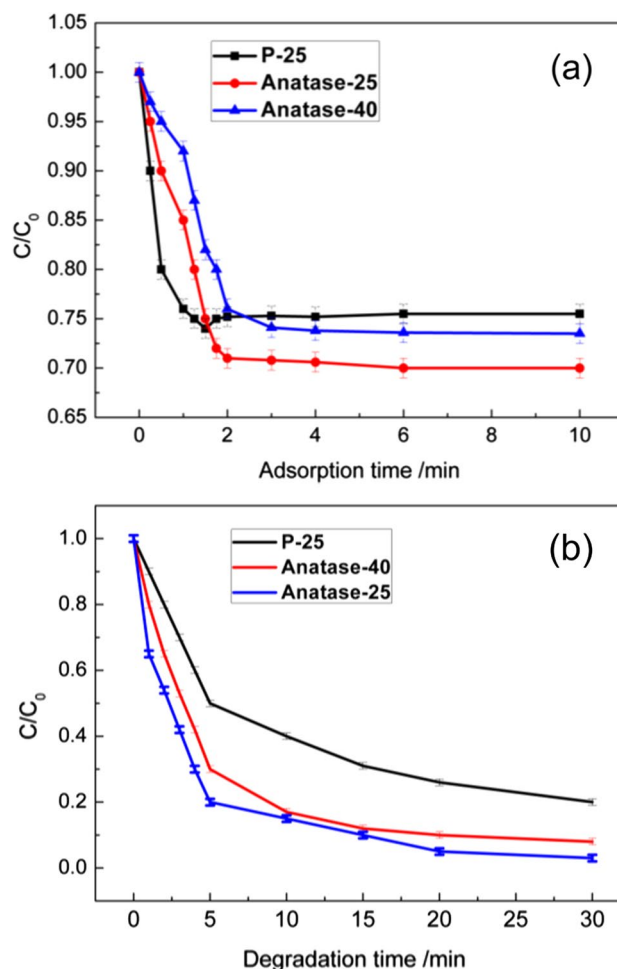


**Fig. 5** Adsorption and photocatalytic degradation of phenol using different photocatalysts (**a** adsorption curves, temperature: 25 °C; **b** degradation curves, temperature: 25 °C, the concentration of phenol: 50 mg/L)

where  $N$  is experimental times;  $k$  is the number of variables;  $C_0$  is the central point of the design.

According to the results in Fig. 5, we choose Anatase-25 as the photocatalyst to test the activity of anatase nano-powders. Table S3 shows the four factors design table for BBD experiments. The experimental data are analyzed by Design-experiment version 8.0.6.1 software. To evaluate the accuracy of the model in the present study, we fit the experimental data and predicted values, which are shown in Fig. 6. The R square of the line is 0.987, which demonstrates that the predicted results are in good agreement with experimental results. The estimated equation for output response  $y$  in terms of coded factors is given as:

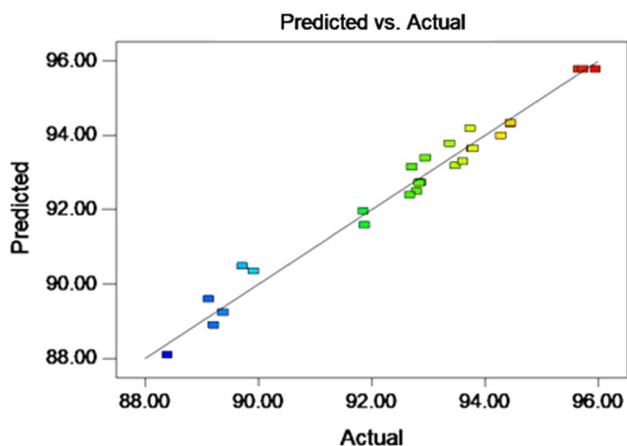


Fig. 6 Predicted reaction rate versus the experimental data

$$\begin{aligned}
 y = & -281.38963 + 2.45722x_1 + 0.095315x_2 + 14.09631x_3 \\
 & - 44.27592x_4 + 5.5E - 006x_1x_2 - 0.051260x_1x_3 \\
 & + 2.75E - 004x_1x_4 + 9.65894E - 017x_2x_3 - 6.05E \\
 & - 004x_2x_4 - 1.1E - 003x_3x_4 - 0.018452x_1^2 - 0.22946x_2^2 \\
 & - 0.22946x_3^2 - 3.53237x_4^2
 \end{aligned} \tag{2}$$

where  $x_1$  is degradation time,  $x_2$  is dosage of  $TiO_2$ ,  $x_3$  is temperature, and  $x_4$  is pH.

The variance of the predicted values is summarized in Table 3,  $p$ -values in Table 3 can be used to identify the significance of each factor, and low  $p$ -value ( $<0.05$ ) implies

that the factor has a significant influence on photocatalytic degradation of phenol. It can be concluded from the Model  $F$  (39.48) and  $p$  ( $<0.0001$ ) values that the model is an ideal way to optimize the photocatalytic degradation of phenol as a function of the selected factors. Lack of fit for  $F$  and  $p$  values are 11.01 and 0.0861, which demonstrates that the regression equation can describe the relationship between response variables and the degradation rates. The  $p$ -value of model ( $p < 0.0001$ ),  $x_1$  ( $p = 0.0013$ ),  $x_2$  ( $p = 0.0255$ ),  $x_4$  ( $p < 0.0001$ ),  $x_1x_3$  ( $p = 0.0001$ ),  $x_1^2$  ( $p < 0.0001$ ),  $x_2^2$  ( $p = 0.0231$ ),  $x_3^2$  ( $p < 0.0001$ ),  $x_4^2$  ( $p < 0.0001$ ) are statistically significant. These results indicate that degradation time and dosage of  $TiO_2$  are critical to the degradation of phenol.

Additionally, pH can influence the behavior of anatase NPs in aqueous suspensions, such as zeta potential and aggregate size. Thus, it can be induced that pH is a key factor for the photocatalytic activity of the nano-powders. This is in agreement with the results presented by Liu et al. (2018). The  $p$ -value of lack of fit was 0.0861, larger than 0.05, indicating a small error between the model and practical experiments. Thus, our model possessed a high fitness toward the degradation results. Additionally, the difference between Adj-R-squared and R-squared is  $0.1377 < 0.2$ , which implies a good relationship between the predicted and experimental values. We can evaluate the effect of the factors by comparing the  $F$ -values of each factor. Thus, the effect of single factor followed the trend:  $pH(x_4, 164.58) > degradation\ time(x_1, 17.47) > dosage$

Table 3 Variance of the results of phenol degradation rate as a response variable

Source	Sum of squares	df	Mean square	F-value	p-value	Remark
Model	122.64	14	8.76	39.48	<0.0001	*
$x_1$	3.88	1	3.88	17.47	0.0013	*
$x_2$	1.44	1	1.44	6.49	0.0255	*
$x_3$	0.35	1	0.35	1.59	0.2314	
$x_4$	36.52	1	36.52	164.58	<0.0001	*
$x_1x_2$	3.025E-005	1	3.025E-005	1.363E-004	0.9909	
$x_1x_3$	6.57	1	6.57	29.61	0.0001	*
$x_1x_4$	3.025E-005	1	3.025E-005	1.363E-004	0.9909	
$x_2x_3$	1.421E-14	1	1.421E-14	6.405E-014	1.0000	
$x_2x_4$	3.66E-003	1	3.66E-003	0.016	0.8999	
$x_3x_4$	3.025E-005	1	3.025E-005	1.363E-004	0.9909	
$x_1^2$	18.16	1	18.16	81.85	<0.0001	*
$x_2^2$	1.5	1	1.5	6.77	0.0231	*
$x_3^2$	10.97	1	10.97	49.44	<0.0001	*
$x_4^2$	66.55	1	66.55	299.93	<0.0001	*
Residual	2.66	12	0.22			
Lack of fit	2.62	10	0.26	11.01	0.0861	
Pure error	0.048	2	0.024			
Total	125.31	26				

\* in the table means significant

of  $\text{TiO}_2(x_2, 6.49) > \text{temperature}(x_3, 1.59)$ . The order of interaction factors was:  $x_1x_3(29.61) > x_2x_4(0.061) > x_1x_4(1.363\text{E}-004) = x_3x_4 = x_1x_2(1.363\text{E}-004) > x_2x_3(6.405\text{E}-014)$ . The Effect of square factors followed the trend:  $x_4^2(299.93) > x_1^2(81.85) > x_3^2(49.44) > x_2^2(6.77)$ . Additionally, the  $R^2$  value of the regression equation is 0.9540, which implies the regression equation can describe 95.40% of the results, and the model used in the present work is fit to predict the photodegradation process of phenol.

To provide a better visualization of the interactions between different experimental factors on the effects of response variables, 3-dimensional response surfaces are performed (Fig. 7a, b, c, d, e and f).

The color in Fig. 7 changes from blue to red represents changes in the photocatalytic degradation rate of phenol from low to high. The plots show the effect of two experimental variables on a response while the other variables are kept constant. Figure 7a shows the effect of degradation time and dosage of  $\text{TiO}_2$  on the degradation rate of phenol (here the temperature is  $27.5^\circ\text{C}$ , and the pH is 6). In single-factor experiments (Fig. 5b), the degradation rate of phenol increases with degradation time, which does not agree with Fig. 7a. A counterintuitive behavior is found: the degradation of phenol did not increase with degradation

of time, this attributes to the interaction between the factors degradation time and dosage of  $\text{TiO}_2$ . Additionally, the degradation of phenol is not very sensitive to the dosage of  $\text{TiO}_2$ , which indicates that  $\text{TiO}_2$  is readily sufficient. Figure 7b shows the simultaneous effect of degradation time and temperature on the degradation of phenol (The dosage of  $\text{TiO}_2$  and pH are  $200\text{ mg/L}$  and  $6.0$ ). The degradation rate neither increases with degradation time nor increases with temperature. The interactions between degradation time and temperature show a critical effect on the degradation of phenol. Figure 7c shows the simultaneous effect of degradation time and pH (the dosage of  $\text{TiO}_2$  and temperature are kept at  $200\text{ mg/L}$  and  $27.5^\circ\text{C}$ ). The high degradation rate region is centered in the middle of the response surface. As summarized in Table 3, the  $p$ -value of  $x_1x_3$  is 0.0001, which demonstrated rather strong interactions between these two factors. Figure 7d shows the effect of the dosage of  $\text{TiO}_2$  and temperature on the degradation of phenol (the degradation time is  $30\text{ min}$ , and the pH is  $6.00$ ). Compared to the dosage of  $\text{TiO}_2$ , the temperature shows less influence on the degradation rate of phenol, which implies dosage of  $\text{TiO}_2$  play a more important role than temperature, this is consistent with Table 3, the dosage of  $\text{TiO}_2$  is a significant factor while the temperature is not significant in the present range. However, this phenomenon may not apply to all degradation experiments. The degradation rate could be very sensitive to temperature. A study presented by Krivec et al. demonstrates that more photocatalysts can be activated at higher temperatures, and thus, degradation of phenol can be enhanced effectively (Krivec et al. 2015). Figure 7e shows the effect of the dosage of  $\text{TiO}_2$  and pH on the degradation of phenol (the degradation time and temperature are kept at  $30\text{ min}$  and  $27.5^\circ\text{C}$ ). Compared with the dosage of  $\text{TiO}_2$ , pH exhibits a sharp effect on the degradation of phenol. A proper explanation of this can be found in Fig. 4 and Table 2. When the pH is close to the isoelectric point, the agglomeration of  $\text{TiO}_2$  NPs is minimized, thereby producing higher photocatalytic activities. The agglomeration size of Anatase-25 is very sensitive to pH. A smaller agglomeration size implies more active sites in the solutions. Consequently, the Anatase-25 shows high photocatalytic activities when the pH is around 6.75. Similarly, the degradation of phenol shows a pH-dependent behavior, which means pH has much more influence than the temperature in Fig. 7(f) (the dosage of  $\text{TiO}_2$  and degradation time are fixed at  $200\text{ mg/L}$  and  $30\text{ min}$ ), simply because pH is a more significant factor than temperature (the results shown in Table 3). According to the model, a degradation rate of 96.086% could be obtained under the following optimal condition: degradation time of  $28.5\text{ min}$ , the dosage of  $\text{TiO}_2$   $211.25\text{ mg/L}$ , degradation temperature  $27.44^\circ\text{C}$ , and pH  $6.22$ . Under the optimal condition, we did experiments using the above optimal condition, and the corresponding degradation rate is 96.35%. Chiou

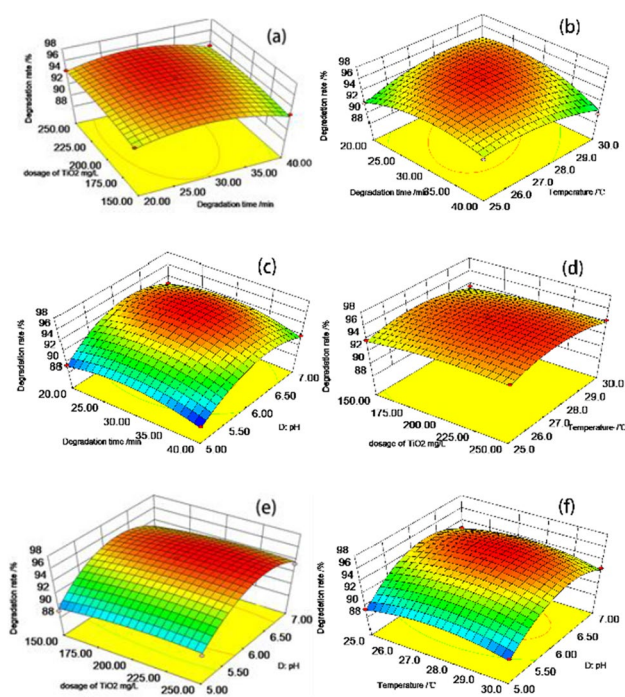


**Fig. 7** Response surface of the effect of different variables on degradation of phenol (a effect of dosage of  $\text{TiO}_2$  and degradation time; b effect of degradation time and temperature, c effect of degradation time and pH, d effect of dosage of  $\text{TiO}_2$  and temperature, e effect of dosage of  $\text{TiO}_2$  and pH, f effect of temperature and pH)



et al. (2007) presented a study using pure anatase and Pr-doped as a photocatalyst to degrade phenol; 40% phenol was degraded after 100 min for the pure anatase sample, while the degradation rate is 96% using Pr-doped sample under the same condition. Yilleng and co-workers (2018) degraded phenol by using Pd-doped TiO<sub>2</sub>. They converted more than 90% phenol after 110-min radiation of visible light. Zamri and Sapawe (2018) reported that a degradation rate of 97% of phenol could be obtained in pH 5 phenol solution after 2 h of visible light irradiation by using electro-synthesized TiO<sub>2</sub>. Compared to the photocatalysts in the literature, the as-prepared sample in this study exhibits a higher activity simply because of the uniform particle size and morphology of the samples produced by the microfluidic method.

Based on the study of this work, microfluidic synthesis of anatase NPs is an ideal alternative to conventional approaches, since the experimental parameters, e.g., mixing rates, flow rates and mixing volumes, can be controlled on the micro/nanoscale, thereby enabling more precise control over particle size of the samples. Additionally, diverse strategies can be achieved on designing of chips on microfluidic synthesizing of NPs, which allows higher mass transfer efficiency than bulk technique. On the other hand, although microfluidic synthesis of anatase NPs is proved to be feasible for fabrication of NPs, further study on controlling of the morphology of the samples and interactions in the microchannels is still in need to better benefit the scientific community of material synthesis.

## Conclusions

In this work, we propose a microfluidic method to synthesize anatase phase NPs with enhanced photocatalytic properties. Orthogonal experimental results demonstrate that the significance of the factors follows the trend: residence time > pH > temperature > channel width > ratio of alcohol in water–ethyl alcohol mixture. The crystallinity of anatase nanoparticles increased with the increase of pH. Zeta potential and agglomerate size of the samples and P-25 in suspensions are measured, and the results demonstrated that the aggregate size of P-25 is much larger than the as-prepared anatase NPs at the same pH. The synthesized anatase nanoparticles exhibit higher photocatalytic activity than commercial P-25. RSM is used to present a panoramic sight of the degradation of phenol under visible-light irradiation. According to the model in RSM, the optimal degradation condition of phenol is degradation time 28.5 min, the dosage of TiO<sub>2</sub> 211.25 mg/L, degradation temperature 27.44 °C, and pH 6.22.

**Supplementary Information** The online version contains supplementary material available at <https://doi.org/10.1007/s11696-023-02736-0>.

**Acknowledgements** The authors gratefully acknowledge the financial support from the Department of education of Liaoning province, China (LJKZ0250).

## Declarations

**Conflicts of interest** There are no conflicts to declare.

## References

- Bendre A, Bhat MP, Lee KH, Altalhi T, Alruqi MA, Kurkuri M (2022) Recent developments in microfluidic technology for synthesis and toxicity-efficiency studies of biomedical nanomaterials. *Mater Today Adv* 13:100205
- Cargnello M, Gordon TR, Murray CB (2014) Solution-phase synthesis of titanium dioxide nanoparticles and nanocrystals. *Chem Rev* 114(19):9319–9345
- Chen X, Mao SS (2007) Titanium dioxide nanomaterials: synthesis, properties, modifications, and applications. *Chem Rev* 107(7):2891–2959
- Chen KH, He Y, Srinivasakannan C, Li SW, Yin SH, Peng JH, Guo SH, Zhang LB (2019) Characterization of the interaction of rare earth elements with P507 in a microfluidic extraction system using spectroscopic analysis. *Chem Eng J* 356:453–460
- Chen H, Dong Z, Yue J (2022) Advances in microfluidic synthesis of solid catalysts. *Powders* 1:155–183
- Chiou CH, Juang RS (2007) Photocatalytic degradation of phenol in aqueous solutions by Pr-doped TiO<sub>2</sub> nanoparticles. *J Hazard Mater* 149(1):1–7
- Dambournet D, Belharouak I, Amine K (2010) Tailored preparation methods of TiO<sub>2</sub> anatase, rutile, brookite: mechanism of formation and electrochemical properties. *Chem Mater* 22(3):1173–1179
- Dar MI, Chandiran AK, Gratzel M, Nazeeruddin MK, Shivashankar SA (2014) Controlled synthesis of TiO<sub>2</sub> nanoparticles and nanospheres using a microwave assisted approach for their application in dye-sensitized solar cells. *J Mater Chem A* 2(6):1662–1667
- Dong DB, Li PJ, Li XJ, Zhao Q, Zhang YQ, Jia CY, Li P (2010) Investigation on the photocatalytic degradation of pyrene on soil surfaces using nanometer anatase TiO<sub>2</sub> under UV irradiation. *J Hazard Mater* 174(1–3):859–863
- Dubey RS, Singh S (2017) Investigation of structural and optical properties of pure and chromium doped TiO<sub>2</sub> nanoparticles prepared by solvothermal method. *Results Phys* 7:1283–1288
- Gao HT, Sui XM, Dai DM, Si CD, Liu GJ (2015) Hierarchical honeycomb anatase TiO<sub>2</sub> with (100) facet: facile hydrothermal preparation and enhanced photocatalytic performance. *J Nanosci Nanotechnol* 15(7):5193–5197
- Gautam A, Kshirsagar A, Biswas R, Banerjee S, Khanna PK (2016) Photodegradation of organic dyes based on anatase and rutile TiO<sub>2</sub> nanoparticles. *RSC Adv* 6(4):2746–2759
- He Y, Pei JN, Srinivasakannan C, Li SW, Peng JH, Guo SH, Zhang LB, Yin S (2018) Extraction of samarium using a serpentine Y-junction microreactor with 2-ethylhexyl phosphonic acid mono-2-ethylhexyl. *Hydrometallurgy* 179:175–180
- Jiang F, Yin SH, Srinivasakannan C, Li SW, Peng JH (2018) Separation of lanthanum and cerium from chloride medium in presence of complexing agent along with EHEHPA (P507) in a serpentine microreactor. *Chem Eng J* 334:2208–2214

- Korosi L, Bognar B, Horvath M, Schneider G, Kovacs J, Scarpellini A, Castelli A, Colombo M, Prato M (2018) Hydrothermal evolution of PF-co-doped TiO<sub>2</sub> nanoparticles and their antibacterial activity against carbapenem-resistant *Klebsiella pneumoniae*. *Appl Catal B-Environ* 231:115–122
- Krivec M, Pohar A, Likozar B, Dragic G (2015) Hydrodynamics, mass transfer, and photocatalytic phenol selective oxidation reaction kinetics in a fixed TiO<sub>2</sub> microreactor. *AIChE J* 61(2):572–581
- Li C, Wang Z, Xie H, Bao J, Wei Y, Lin B, Liu Z (2022) Facile precipitation microfluidic synthesis of monodisperse and inorganic hollow microspheres for photocatalysis. *J Chem Technol Biotechnol* 97:1215–1223
- Lin SH, Chiou CH, Chang CK, Juang RS (2011) Photocatalytic degradation of phenol on different phases of TiO<sub>2</sub> particles in aqueous suspensions under UV irradiation. *J Environ Manage* 92(12):3098–3104
- Liu XH, Liu Y, Lu SY, Guo W, Xi BD (2018) Performance and mechanism into TiO<sub>2</sub>/Zeolite composites for sulfadiazine adsorption and photodegradation. *Chem Eng J* 350:131–147
- Lujan-Moreno GA, Howard PR, Rojas OG, Montgomery DC (2018) Design of experiments and response surface methodology to tune machine learning hyperparameters, with a random forest case study. *Expert Syst Appl* 109:195–205
- Monfared AH, Jamshidi M (2019) Effects of photocatalytic activity of nano TiO<sub>2</sub> and PANi/TiO<sub>2</sub> nanocomposite on the physical/mechanical performances of acrylic pseudo paints. *Prog Org Coat* 136:105300
- Mou J, Ren Y, Wang J, Wang C, Zou Y, Lou K, Zheng Z, Zhang D (2022) Nickel oxide nanoparticle synthesis and photocatalytic applications: evolution from conventional methods to novel microfluidic approaches. *Microfluid Nanofluid* 26:25
- Nithya N, Bhoopathi G, Magesh G, Kumar CDN (2018) Neodymium doped TiO<sub>2</sub> nanoparticles by sol-gel method for antibacterial and photocatalytic activity. *Mater Sci Semicond Process* 83:70–82
- Pandit P, Rananaware P, D'SouzaKurkuriBrahmkhatra AMDV (2022) Functionalized diatom biosilica decorated with nanoparticles: synthesis, characterization, catalytic oxidation, and dye scavenging applications. *J Porous Mater* 29:1369–1383
- Pei JN, Zhou JW, Jiang F, Chen KH, Yin SH, Zhang LB, Peng JH, Lin YP (2018) Kinetics analysis of the forward extraction of cerium(III) by D2EHPA from chloride medium in the presence of two complexing agents using a constant interfacial area cell with laminar flow. *Green Process Synth* 7(4):380–386
- Priest C, Zhou JF, Sedev R, Ralston J, Aota A, Mawatari K, Kitamori T (2011) Microfluidic extraction of copper from particle-laden solutions. *Int J Miner Process* 98(3–4):168–173
- Tabaei HSM, Kazemeini M, Fattahi M (2012) Preparation and characterization of visible light sensitive nano titanium dioxide photocatalyst. *Sci Iran* 19(6):1626–1631
- Testino A, Bellobono IR, Buscaglia V, Canevali C, D'Arienzo M, Polizzi S, Scotti R, Morazzoni F (2007) Optimizing the photocatalytic properties of hydrothermal TiO<sub>2</sub> by the control of phase composition and particle morphology. A systematic approach. *J Am Chem Soc* 129(12):3564–3575
- Wang CY, Rabani J, Bahnemann DW, Dohrmann JK (2002) Photonic efficiency and quantum yield of formaldehyde formation from methanol in the presence of various TiO<sub>2</sub> photocatalysts. *J Photochem Photobiol, A* 148(1):169–176
- Yilleng MT, Gimba EC, Ndukwe GI, Bugaje IM, Rooney DW, Man-yar HG (2018) Batch to continuous photocatalytic degradation of phenol using TiO<sub>2</sub> and Au-Pd nanoparticles supported on TiO<sub>2</sub>. *J Environ Chem Eng* 6(5):6382–6389
- Yin SH, Chen KH, Srinivasakannan C, Guo SH, Li SW, Peng JH, Zhang LB (2018) Enhancing recovery of ammonia from rare earth wastewater by air stripping combination of microwave heating and high gravity technology. *Chem Eng J* 337:515–521
- Yuenyongsuwan J, Nithiyakorn N, Sabkird P, O'Rear EA, Pongprayoon T (2018) Surfactant effect on phase-controlled synthesis and photocatalyst property of TiO<sub>2</sub> nanoparticles. *Mater Chem Phys* 214:330–336
- Zamri M, Sapawe N (2018) Performance studies of electrobiosynthesis of titanium dioxide nanoparticles (TiO<sub>2</sub>) for phenol degradation. *Mater Today Proc* 5(10):21797–21801
- Zhang WF, Chen JR, Lin G, Zhang LB (2017) Experimental optimization of microwave drying zinc oxide leach residues by response surface methodology. *Green Process Synth* 6(5):523–532
- Zhang JJ, Li L, Li YX, Yang CF (2018) H<sub>2</sub>SO<sub>4</sub> induced mesoporous TiO<sub>2</sub> nano-photocatalyst synthesized free of template under microwave. *Powder Technol* 335:54–61
- Zhou SF, Hong ZL, Zhao FR, Fan XP, Wang MQ (2006) Characterization of optical response properties for a nanosized TiO<sub>2</sub> with visible-light response. *J Inorg Mater* 21(4):783–788

**Publisher's Note** Springer Nature remains neutral with regard to jurisdictional claims in published maps and institutional affiliations.

Springer Nature or its licensor (e.g. a society or other partner) holds exclusive rights to this article under a publishing agreement with the author(s) or other rightsholder(s); author self-archiving of the accepted manuscript version of this article is solely governed by the terms of such publishing agreement and applicable law.